

## Effect of a Variable Eddy Transfer Coefficient in an Eddy-Permitting Model of the Subpolar North Atlantic Ocean

DANIEL DEACU AND PAUL G. MYERS

*Department of Earth and Atmospheric Sciences, University of Alberta, Edmonton, Alberta, Canada*

(Manuscript received 23 May 2003, in final form 27 July 2004)

### ABSTRACT

The effect of using a variable eddy transfer coefficient for the Gent–McWilliams (GM) parameterization in a  $(1/3)^\circ$ -resolution ocean model of the subpolar North Atlantic Ocean is investigated. Results from four experiments with different implementations of this coefficient are compared among themselves as well as with two control experiments. A series of improvements have been obtained in all of the experiments that use a low level of explicit horizontal tracer diffusion. These include a better representation of the overflow waters originating from the Nordic seas, leading to a more realistic deep western boundary current and to increased eddy activity in the deep ocean in the eastern North Atlantic. In the same experiments, the GM velocities “help” the Labrador Sea Water to spread from the deep convection region to the currents that surround it without incurring significant spurious diapycnal mixing. Thus, two classical pathways for the spreading of this water are established. Moreover, the simulated Labrador Current and the near-surface circulation in the eastern North Atlantic are in better agreement with flow patterns inferred from observations. The increased release of available potential energy obtained in the experiments with variable eddy transfer coefficients is responsible for the simulation of a flow that varies less in time. An overly strong countercurrent still occurs in the Labrador Sea in these experiments, and it has a negative impact on the pathway of the North Atlantic Current in the “Northwest Corner” and on the hydrography of the Labrador Sea. Nonetheless and overall, the use of the variable eddy transfer coefficient has led to better representations of the general circulation and hydrography in the subpolar North Atlantic.

### 1. Introduction

The effects of baroclinic eddies on tracers need to be parameterized in coarse-resolution ocean models. Gent and McWilliams (1990) proposed a mesoscale eddy parameterization scheme (hereinafter denoted by GM) for  $z$ -coordinate models that can be implemented by adding a so-called bolus velocity (Gent et al. 1995) to the mean transport velocity employed for the advection terms in the tracer equations. The net effect of this eddy-induced velocity is expected to be that of stirring tracers quasi-adiabatically along isopycnal/isoneutral surfaces, similar to the stirring produced by mesoscale eddies. Numerous studies have shown that the GM parameterization leads to improved model fields in coarse-resolution models, including enhanced northward transport of heat in the North Atlantic Ocean, sharper thermoclines, and cooler deep oceans (Danabasoglu et al. 1994; Danabasoglu and McWilliams 1995; Böning et al. 1995). These improvements resulted from

simultaneous use of the GM scheme and a low, or even zero, horizontal diffusion, which reduces considerably the spurious diapycnal mixing and the ensuing spurious upwelling (Böning et al. 1995).

Simulations from an eddy-permitting  $[(1/3)^\circ$  resolution]  $z$ -coordinate model of the North Atlantic reported by Willebrand et al. (2001) showed that the unphysical diapycnal upwelling in the western boundary current region was the result of the tracer diffusion by means of the biharmonic horizontal diffusion scheme. The authors conclude that a nondiffusive/adiabatic scheme for tracer stirring and mixing might preclude this unwanted effect even in the eddy-permitting regime, in a manner similar to that in non-eddy-resolving models. An example showing that the GM scheme may be beneficial in eddy-permitting models has been reported by Haines and Wu (1998), in which it improved the dispersal of the Levantine Intermediate Water in a model of the Mediterranean Sea. Even in the eddy-resolving regime, Roberts and Marshall (1998) have argued that adiabatic dissipation schemes are still required because significant spurious diapycnal mixing is generated by horizontal tracer diffusion schemes; Maltrud and McClean (2005) have mentioned that an adiabatic eddy mixing scheme could improve simulations with their  $(1/10)^\circ$  global ocean model.

---

*Corresponding author address:* Daniel Deacu, Department of Earth and Atmospheric Sciences, 1-26 Earth Sciences Bldg., University of Alberta, Edmonton, AB T6G 2E3, Canada.  
E-mail: ddeacu@ualberta.ca

In all of the listed studies that used the GM scheme (and many others), the strength of the eddy stirring of tracers was represented by a constant eddy transfer coefficient. England and Holloway (1998) reported negative effects when a relatively large value of this coefficient,  $10^7 \text{ cm}^2 \text{ s}^{-1}$ , was used everywhere in a series of North Atlantic simulations, and they suggested that a spatially and temporally varying coefficient could be a remedy. A similar suggestion has been made by Beismann and Redler (2003), who found that the GM scheme with a constant eddy transfer coefficient led to an unrealistic pathway of the North Atlantic Deep Water in their model.

To take into account the inherent variability of the eddy-induced tracer transport in oceanic flows, Visbeck et al. (1997, hereinafter referred to as VMHS) proposed a method to calculate a variable eddy transfer coefficient that can be used with the GM scheme in coarse-resolution ocean models. This coefficient is assumed to be proportional to the Eady growth rate of the unstable baroclinic waves  $T^{-1}$ , given by

$$T^{-1} = \frac{f}{\sqrt{\text{Ri}}}, \quad (1)$$

and to the square of a length scale  $L$  of the baroclinic region. Its expression is

$$k = \alpha T^{-1} L^2, \quad (2)$$

where  $f$  is the Coriolis parameter,  $\text{Ri}$  is the large-scale Richardson number, and  $\alpha$  is a constant equal to 0.015.

Bryan et al. (1999) compared predictions of the magnitude of the bolus velocity yielded by the GM scheme employing a constant eddy mixing coefficient, a VMHS-like coefficient, and the variable eddy coefficient formulation of Held and Larichev (1996), with magnitudes from diagnostic calculations performed with their eddy-permitting model outputs. They found that the prediction with the VMHS-like coefficient given by

$$k = \mu T^{-1} \lambda^2, \quad (3)$$

where  $\mu$  is a constant equal to 0.13 and  $\lambda$  is the local Rossby radius of deformation, was the best fit to the model. Wright (1997) also found that the VMHS coefficient led to improvements in their  $1.25^\circ$ -resolution model as compared with simulations with a constant eddy coefficient.

Gent et al. (2002) used the GM parameterization with the VMHS coefficient in an eddy-permitting global ocean model (having an average horizontal resolution of  $\sim 0.7^\circ$ ). Although they found that the VMHS scheme only produced minor differences in the global fields as compared with a constant eddy coefficient, the authors concluded that significant local differences could occur in regions where the variable eddy coefficient becomes larger, such as the Antarctic Circumpolar Current and the northern North Atlantic.

Observations conducted in the Labrador Sea have revealed the ubiquitous presence of geostrophic eddies with a length scale of about 10 km (approximately equal to typical Rossby radius of deformation values for that region) and baroclinic instability in the convection region (The Lab Sea Group 1998). Eddy-permitting ocean models are a class of models that can simulate large eddies but do not allow for the geostrophic eddy field to be fully resolved because their horizontal grid spacing is still larger than the Rossby radius of deformation. This inability to resolve the Rossby radius is more preponderant toward high latitudes as the ratio of the local horizontal grid spacing to the local Rossby radius increases. Therefore, processes such as meandering of baroclinically unstable currents leading to a growth phase and the ultimate spawning of a baroclinic eddy are not simulated adequately. It is very likely that, because of constraints imposed by the grid size, a resolved baroclinic eddy is only spawned after certain thresholds for available potential energy and velocity shear have been exceeded. It may be, for the case of frontal regions, that some large amount of available potential energy needs to be accumulated before it can be released by the shedding of baroclinic eddies of a scale sufficiently large to be resolved by the model grid. Sudden release of available potential energy can generate very energetic eddies that may have a negative impact on the model circulation in a region. Because the transport of tracers by the unresolved mesoscale eddies still needs to be parameterized in eddy-permitting models, the option of an eddy transfer coefficient varying according to the local susceptibility to baroclinic instability should have a positive contribution to the removal of available potential energy and thus lead to more realistic simulations.

Recent simulations performed with an eddy-permitting model [ $(1/3)^\circ$  resolution] of the subpolar North Atlantic (Myers 2002) showed that the use of a better topographic representation based on the partial cell approach of Adcroft et al. (1997) leads to an improved representation of the circulation in that region. However, the changes to the circulation caused the model salinity in the Labrador Sea to drift to unrealistically high values. An overly strong Labrador Sea countercurrent caused excessive entrainment of high-salinity water from the North Atlantic Current (NAC) into the Labrador Sea (Myers and Deacu 2004) and thus occasioned the salinity drift. Myers and Deacu (2004) suggested that increased baroclinic eddy activity in the partial cell simulation might have been responsible for the acceleration of the countercurrent.

With the importance of eddy activity and instability processes in the simulations of Myers and Deacu (2004), a natural extension of that study was to consider the use of the GM scheme with VMHS-like eddy transfer coefficients. One result that might be expected would be a decreased baroclinic eddy activity due to an enhanced release of available potential energy in baro-

clinically unstable regions (e.g., frontal and deep-convection regions), because a very small value of the eddy transfer coefficient ( $2.0 \times 10^5 \text{ cm}^2 \text{ s}^{-1}$ ) was used in the previous study. In addition, it was hoped that the improved representation of the eddy processes could reduce spurious diapycnal mixing through a drastic decrease of the horizontal tracer diffusivity.

Eddy-permitting ocean general circulation models are increasingly being used for climate studies (e.g., Roberts et al. 2004), and skillful eddy parameterizations are needed for these models to yield more accurate simulations (Gent et al. 1999). The main objective of the study presented in this paper is to investigate the effect of the use of the GM scheme with a variable eddy transfer coefficient, combined with a low level of horizontal diffusion, in simulations with an eddy-permitting model of the subpolar North Atlantic. To assess the relative contribution of using variable eddy transfer coefficients and reducing the explicit horizontal diffusion, we compare results from experiments that employ a spatially and temporally variable eddy transfer coefficient with results from two control experiments with constant values for this coefficient. One of the control experiments uses a value for the eddy transfer coefficient obtained as a spatial and time average of the eddy coefficient field from one of the experiments in which it is variable and uses a small value for the biharmonic horizontal diffusion coefficient. The other one uses the settings of the model from previous studies—that is, a lower value for the eddy transfer coefficient and a typical value of the biharmonic horizontal diffusion coefficient for the eddy-permitting regime.

The experiments with a variable eddy transfer coefficient correspond to two different implementations of the expressions (2) and (3) of this coefficient. The implementations are described in section 2, and more detail on the ocean model is given in section 3. Results from all experiments are presented and discussed in section 4. The conclusions are provided in section 5.

## 2. On the implementation of the VMHS eddy transfer coefficient in an eddy-permitting ocean circulation model

In an eddy-permitting ocean model, large geostrophic eddies can be simulated and their effect on tracers need not be parameterized. Therefore, the attention should be focused on parameterizing the smaller baroclinic eddies that cannot be explicitly resolved. This study makes use of the assumption that, when using (2), this can be achieved to some extent by limiting the length scale  $L$  of the baroclinic region such that its upper bound is comparable to the length scale of the smallest eddies resolved by the model. Visbeck et al. (1997) devised a method of determining  $L$  based on the discrete field of the growth rate. Moreover, it is for this particular method that they found a value of 0.015 for the “universal” constant  $\alpha$ . Because this value was

considered by VMHS to be appropriate even for parameterizing baroclinic regions with relatively small length scales (e.g., see their convective chimney case), which an eddy-permitting model cannot resolve at high latitudes, we chose to leave it unchanged.

To avoid overparameterizing the effects of the resolved eddies, we set the upper limit for  $L$  to  $1^\circ$  of longitude, that is, 3 times the meridional grid size, which is constant in our model. Although this choice is not physically sound, it can be related to the minimum number of grid points in both zonal and meridional directions that is required to represent an eddy on the horizontal grid properly. The growth rate is precisely defined by (1), but there is no such formal definition for the length scale  $L$ . We use the algorithm employed by the Modular Ocean Model, version 3 (MOM3; Pacanowski and Griffies 1998) and attributed to the Hadley Centre, to determine this length scale based on the previously calculated growth-rate field. The details are given in the appendix. When calculating the eddy transfer coefficient with formula (3), there is no need to limit  $\lambda$  (local Rossby radius) because it is at the lower end of the length-scale range of mesoscale eddies (whose scale is typically 3–4 $\lambda$ ; Stammer 1998), that is, exactly in the subrange of the mesoscale eddies unresolved by the eddy-permitting ocean models.

Note that, because  $\lambda$  does not require any input on setting its upper limit, one may find (3) preferable over (2) for computing the eddy transfer coefficient at different resolutions in the eddy-permitting regime. However, the limitation imposed on  $L$  leads to an overall decrease of this coefficient when increasing the resolution, which is more consistent with a narrower size range of the unresolved mesoscale eddies. No studies have been performed on the sensitivity of the eddy transfer coefficient given by the two formulas to the horizontal grid spacing. One way of addressing the possible overparameterization of the effect of the mesoscale eddies in the eddy-permitting regime when using either (2) or (3) is to tune the constants  $\alpha$  and  $\mu$ , respectively.

The expression of the Richardson number in (1) is

$$\text{Ri} = \frac{N^2}{\left(\frac{du}{dz}\right)^2 + \left(\frac{dv}{dz}\right)^2}, \quad (4)$$

where  $N$  is the buoyancy frequency given by  $N^2 = (-g/\rho_0)d\rho/dz$ ,  $g$  is the gravitational acceleration,  $\rho$  is the locally referenced density,  $\rho_0$  is a reference density (with a value of  $1 \text{ g cm}^{-3}$ ), and  $u$  and  $v$  are the horizontal components of the velocity vector. Two methods for calculating  $\text{Ri}$  have been considered. One of them (hereinafter referred to as STRAT) follows the original VMHS approach, in which the velocity shear is expressed as a function of horizontal density gradients. The other (denoted by SHEAR) is similar to an implementation used at the Hadley Centre and directly cal-

culates the velocity shear using the total velocity field, which is a prognostic variable.

In STRAT, the large-scale Richardson number  $Ri$  is calculated assuming that the mesoscale eddy field is quasigeostrophic, which implies the existence of the thermal-wind balance. Therefore, the vertical velocity shear can be expressed in terms of horizontal density gradients. In this case,  $Ri$  becomes

$$Ri = \left( \frac{f}{NS_{\rho\theta}} \right)^2, \quad (5)$$

where  $S_{\rho\theta}$  stands for the isopycnal slope. As a consequence, the reciprocal of the time scale (i.e., the growth rate) will depend on density gradients only:

$$T^{-1} = N|S_{\rho\theta}|. \quad (6)$$

The right-hand side of (6) is evaluated as an average for each vertical column over a depth interval in which baroclinic eddies are most likely to occur. The lower and upper limits of this interval have been set to 100 and 2000 m, respectively, as suggested by Treguier et al. (1997). Notice that, because of vertical averaging, the computed growth rate will not vary in the vertical direction.

The SHEAR implementation makes direct use of (1) to compute the growth rate. The model directly evaluates the Richardson number from (4) as a depth average for each vertical column. The depth limits are the same as those given in the discussion of the STRAT approach. The two implementations have been used for computing the eddy transfer coefficient using both (2) and (3). Four experiments have been performed, one for each combination of implementation and expression for the eddy transfer coefficient  $k$ . Those with  $k$  given by (2) will be referred to as STRAT<sub>L</sub> and SHEAR<sub>L</sub>, whereas STRAT<sub>λ</sub> and SHEAR<sub>λ</sub> will denote those with  $k$  calculated with (3).

Isopycnal surfaces can be very steep in some regions of the ocean (e.g., mixed layer, frontal, and deep convection regions). Many of the commonly used isopycnal diffusion schemes (Cox 1987) are only valid for small isopycnal slopes, because they are small-slope approximations of a general scheme proposed by Redi (1982). The limitation of isopycnal slopes to small values (e.g., 0.01; Danabasoglu et al. (1994), also required for numerical stability (Cox 1987), leads to significant spurious diapycnal fluxes of density (Mathieu 1998). Therefore, in the absence of physical reasons for using the same slope limitation for the GM scheme (Mathieu 1998), we have relaxed these limiting constraints, such that slopes of up to a maximum absolute value of 100 (corresponding to an almost vertical surface, with a maximum angle of 89.4°) are used when calculating bolus velocity.

Because the  $u$  and  $v$  components of this velocity are proportional to the vertical derivatives of the  $x$  and  $y$  components of the isoneutral slope vector, respectively,

very large values result in regions in which these slopes exhibit a sudden decrease/increase. For example, this effect can happen at the base of the mixed layer and can generate spurious deepening (effect noticed in one of our test experiments). To reduce the amplitude of these negative effects, as well as to keep bolus velocity values within the range of values believed to occur in the ocean, that is, less than 20 cm s<sup>-1</sup> (Mathieu 1998), tapering of vertical derivatives of isopycnal slopes is necessary. A tapering formula of the form proposed by Gerdes et al. (1991) for isopycnal slopes has been used for tapering vertical derivatives of isopycnal slopes greater than a prescribed maximum value  $slpderiv_{max} = 10^{-6}$  cm<sup>-1</sup>. The tapering coefficient is calculated with the formula

$$taper = \left( \frac{slpderiv_{max}}{|dS_{\rho\theta}/dz|} \right)^3, \quad (7)$$

where  $dS_{\rho\theta}/dz$  is the vertical derivative of the isopycnal slope. Thus, if the computed  $dS_{\rho\theta}/dz$  is larger than  $slpderiv_{max}$  then it will be reduced by multiplication by “taper.” Note that for a maximum allowable eddy transfer coefficient of 10<sup>7</sup> cm<sup>2</sup> s<sup>-1</sup>—Visbeck et al. (1997) found a value of 5 × 10<sup>6</sup> cm<sup>2</sup> s<sup>-1</sup> to be representative for the frontal region in their study—a maximum value of 10 cm s<sup>-1</sup> is obtained for the horizontal components of the bolus velocity when the vertical derivative of isopycnal slopes is equal to the prescribed maximum value.

A baroclinic time step of 1800 s has been used for all of the model runs presented in this paper. In this case, the eddy transfer coefficient fields need not be updated during every baroclinic time step. The updating frequency must be dependent on the growth rate ( $T^{-1}$ ) field dynamics (Visbeck et al. 1997). We have chosen a simplified approach whereby the updating takes place after a prescribed number of baroclinic time steps. For a baroclinic time step of 1800 s, this value has been set equal to 24, which means that the eddy transfer coefficient is calculated and updated every 12 h. The central processing unit (CPU) cost associated with this procedure is negligible.

The minimum value of the eddy coefficient has been set equal to 5 × 10<sup>5</sup> cm<sup>2</sup> s<sup>-1</sup>, which is much smaller than the minimum value of 3 × 10<sup>6</sup> cm<sup>2</sup> s<sup>-1</sup> chosen by Wright (1997) to remove noise in his simulations with one of the Hadley Centre’s ocean models. We chose a smaller value to let the eddy transfer coefficient vary toward low values and thus enlarge its range. We also employed a low background horizontal diffusion to help to remove noise in the tracer fields.

### 3. Model

The Subpolar Ocean Model (SPOM) is a regional configuration of the Modular Ocean Model array processor version (MOMA) set up specifically for process

and sensitivity studies of ocean-variability questions in the subpolar North Atlantic. The original model formulation is based on a Bryan–Cox–Semtner type ocean general circulation model using the inviscid version of the Killworth et al. (1991) free-surface scheme. The model is briefly described in the following. The reader will find more details in Myers (2002).

The model has a nonisotropic horizontal resolution of  $(1/3)^\circ \times (1/3)^\circ$ , and its computational domain covers the region of the North Atlantic from  $38^\circ$  to  $70^\circ\text{N}$ . At a given latitude, the grid spacing in the zonal direction is equal to that at the equator [that corresponds to  $(1/3)^\circ$ ] multiplied by cosine of that latitude. The meridional grid spacing remains constant over the grid. The model has 36 levels, unevenly spaced in the vertical direction, with greater resolution in the upper water column. The topography was taken from the  $(1/12)^\circ$  Earth Topography—5 Minute (ETOPO5; NOAA 1988) dataset and then linearly interpolated to the model's resolution. Actual depths are used with the model's incorporation of a partial cell formulation (other than ensuring no partially filled level has less than 10 m of water in it).

The standard settings for our first control run specify a biharmonic horizontal viscosity coefficient  $A_h = 7.5 \times 10^{18} \text{ cm}^4 \text{ s}^{-1}$  and a biharmonic horizontal diffusion coefficient  $K_h = 7.5 \times 10^{18} \text{ cm}^4 \text{ s}^{-1}$ . The vertical viscosity coefficient is  $A_v = 1.5 \text{ cm}^2 \text{ s}^{-1}$ , and the vertical diffusion coefficient is  $K_v = 0.3 \text{ cm}^2 \text{ s}^{-1}$ . The constant value of the eddy transfer coefficient used by the GM scheme is  $2.0 \times 10^5 \text{ cm}^2 \text{ s}^{-1}$ .

Convective adjustment is performed using the complete convection scheme of Rahmstorf (1993). A momentum flux given by a quadratic friction law is applied at the bottom. SPOM does not currently incorporate a bottom boundary layer (BBL) parameterization such as that of Beckmann and Döscher (1997), which was found to significantly improve the downslope flow of the overflow waters in the North Atlantic.

The southern boundary is open, and restoring buffer zones are included along the model's closed northern boundaries. The open boundary formulation is based on the formulation of Stevens (1991), modified with a flow relaxation scheme that restores the sea surface height to a reference state [based on calculations from the diagnostic model of Myers and Weaver (1995)]. Data along the southern boundary are taken from Grey and Haines (1999). More details on the open boundary condition can be found in Myers (2002).

Monthly mean climatological forcing for both the tracers and the winds is applied at the surface. The surface temperature and salinity are relaxed to monthly mean data taken from the NODC (1994) data atlas, with a hard restoring time scale of 2 h. As discussed in Myers (2002), this choice is made to fix the potential water formation regions while leaving the basin interior free to evolve. This restoring boundary condition also constrains the properties of the newly formed waters. Surface momentum fluxes are provided by the monthly

climatology of Trenberth et al. (1990), averaged over the period 1980–86. The model initial conditions are taken from the NODC (1994) dataset, linearly interpolated to the model grid and depth levels.

#### 4. Results and discussion

Results from experiments employing constant and variable eddy transfer coefficients are presented and discussed in this section. For each of them, the model has been started from rest and integrated over a period of 14 yr. The constant values and value ranges for the tracer mixing parameters used in these experiments and in the control experiments are given in Table 1.

Although the following analysis covers the subpolar North Atlantic, the attention is focused on the Labrador Sea region, for which a more detailed comparison with observations and other model studies is provided. There are many similarities among the results obtained from the experiments with variable eddy transfer coefficients. Therefore, in many situations, only results from one of these will be compared with those from the two control experiments.

##### a. Energetics

Higher values of the domain-averaged instantaneous kinetic energy (not shown) reveal that the circulation is generally more energetic in the experiments with low horizontal diffusion. The only exception is  $\text{STRAT}_\lambda$ , in which values similar to those from  $\text{CONTROL}_S$  have been obtained. Values of the mean kinetic energy (MKE), kinetic energy of the mean flow (KEM), and eddy kinetic energy (EKE) per unit mass, for the all of the experiments, are presented in Table 2. These energies are defined as follows:

$$\text{KEM} = \int_V \frac{1}{2} (\bar{u}^2 + \bar{v}^2) dV / \int_V dV, \quad (8)$$

$$\text{EKE} = \int_V \frac{1}{2} (\overline{u'^2} + \overline{v'^2}) dV / \int_V dV, \quad \text{and} \quad (9)$$

$$\text{MKE} = \text{KEM} + \text{EKE}, \quad (10)$$

TABLE 1. Experiments and values of tracer mixing coefficients. Here,  $K_h$  is the biharmonic horizontal diffusion coefficient and  $k$  is the eddy transfer coefficient.

Expt	$K_h$ ( $\times 10^{14} \text{ cm}^4 \text{ s}^{-1}$ )	$k$ ( $\times 10^6 \text{ cm}^2 \text{ s}^{-1}$ )
$\text{CONTROL}_S$	$7.5 \times 10^4$	0.2
$\text{CONTROL}_{\text{AVG}}$	7.5	2.74*
$\text{STRAT}_L$	7.5	0.5–10.0
$\text{SHEAR}_L$	7.5	0.5–10.0
$\text{STRAT}_\lambda$	7.5	0.5–10.0
$\text{SHEAR}_\lambda$	7.5	0.5–10.0

\* This value is the spatial and temporal average of the eddy transfer coefficient calculated over the last 4 yr of the integration in the  $\text{SHEAR}_\lambda$  experiment.

TABLE 2. Domain- and time-averaged kinetic energies and eddy transfer coefficients (calculated over the last 4 yr of integration), and maximum overturning streamfunction at 40°N. KEM is kinetic energy of the mean flow, EKE is eddy kinetic energy, MKE is mean kinetic energy,  $k$  is eddy transfer coefficient, and MOSF is maximum value of the meridional overturning streamfunction at 40°N calculated from the mean velocity field.

Expt	KEM ( $\text{cm}^2 \text{s}^{-2}$ )	EKE ( $\text{cm}^2 \text{s}^{-2}$ )	MKE = KEM + EKE ( $\text{cm}^2 \text{s}^{-2}$ )	EKE/KEM	$k$ ( $\times 10^6 \text{cm}^2 \text{s}^{-1}$ )	MOSF (Sv)
CONTROL <sub>S</sub>	8.5	12.3	20.8	1.45	0.20	19
CONTROL <sub>AVG</sub>	18.7	10.1	28.8	0.54	2.74	41
STRAT <sub>L</sub>	17.5	7.0	24.5	0.40	2.26	34
SHEAR <sub>L</sub>	17.7	9.9	27.6	0.56	1.44	36
STRAT <sub><math>\lambda</math></sub>	15.1	4.9	20.0	0.32	3.67	34
SHEAR <sub><math>\lambda</math></sub>	15.7	7.0	22.7	0.45	2.74	32

where  $\bar{u}$  and  $\bar{v}$  are time-mean values of the velocity components  $u$  and  $v$ , respectively, with  $u' = u - \bar{u}$  and  $v' = v - \bar{v}$ . The time-mean values, as with all of the time-mean fields presented henceforth, have been obtained as time averages over the last 4 yr of integration (years 11–14).

Although EKE is diminished in the experiments with variable eddy transfer coefficients, indicating a decreased variability of the flow, KEM is almost double that in CONTROL<sub>S</sub> and is thus responsible for larger values of MKE (Table 2). The enhanced release of available potential energy in regions where the eddy transfer coefficient takes high values (e.g., off Flemish Cap and the frontal region along the Labrador slope) reduces the level of baroclinic instability and is largely responsible for the significant reduction of the variability of the flow. For example, lower EKE values are obtained in these experiments along the pathway of the NAC, especially around Flemish Cap. In this region known for its high eddy variability and baroclinic instability, the maximum EKE value drops from approximately  $700 \text{cm}^2 \text{s}^{-2}$  at 52-m depth in CONTROL<sub>S</sub> to approximately  $500 \text{cm}^2 \text{s}^{-2}$  in SHEAR<sub>L</sub> and approximately  $420 \text{cm}^2 \text{s}^{-2}$  in SHEAR <sub>$\lambda$</sub> . As discussed in Myers and Deacu (2004), which was based on an experiment similar to CONTROL<sub>S</sub>, the higher EKE values in the partial cell model formulation were in a better agreement with float-based observations. Thus, one of the improvements brought about by the more accurate representation of the bottom topography has been partly lost in CONTROL<sub>AVG</sub> and in the experiments with variable eddy transfer coefficients. This result may be regarded as an undesirable side effect, because ocean modelers strive to obtain an increased and thus more realistic mesoscale eddy activity. Nonetheless, this apparent shortcoming offers the possibility to increase the eddy variability through a reduction of the horizontal viscosity coefficient without compromising the model's numerical stability. Preliminary results from a simulation with a biharmonic horizontal viscosity coefficient,  $7.5 \times 10^{17} \text{cm}^4 \text{s}^{-1}$ , that is one order of magnitude lower have shown that this goal is achievable, although we have not examined this experiment in detail.

The most energetic flow occurs in CONTROL<sub>AVG</sub>.

Its high KEM and low EKE/KEM regime signals a potential resemblance to the flows simulated in the variable eddy transfer coefficient experiments. In some of the experiments, higher MKE values than that in CONTROL<sub>S</sub> may be noted, despite the horizontal and vertical viscosity coefficients remaining unchanged. This result may be explained in part by the reduced viscous dissipation of momentum due to the reduced velocity shear that characterizes the less-variable flows in these experiments. It may also be related to the improved spreading of dense waters in the deep ocean, which acts to accelerate the meridional overturning circulation (see section 4c on overflow waters). The relatively lower values of EKE and EKE/KEM in STRAT <sub>$\lambda$</sub>  and SHEAR <sub>$\lambda$</sub>  mainly originate from the path of the NAC near Grand Banks and Flemish Cap. It is here that the eddy transfer coefficient takes larger values in these experiments in comparison with those in STRAT<sub>L</sub> and SHEAR<sub>L</sub>.

An important result obtained in the experiments with variable eddy transfer coefficients is the increased eddy activity in the deep ocean, where eddy-permitting models usually fail to generate EKE values that are close to values estimated from observations (Smith et al. 2000). Sections of EKE at 48°N (Fig. 1) show that in both CONTROL<sub>S</sub> and CONTROL<sub>AVG</sub> the EKE values in the eastern basin are below  $1 \text{cm}^2 \text{s}^{-2}$ , whereas EKE intensifies at depth, reaching  $5 \text{cm}^2 \text{s}^{-2}$  on the eastern flank of the Mid-Atlantic Ridge (MAR) in SHEAR<sub>L</sub>, which compares very well to values estimated from moored current meters (Colin de Verdière et al. 1989) and to predictions provided by higher-resolution models (Smith et al. 2000). Similar values have been obtained in STRAT<sub>L</sub> and SHEAR <sub>$\lambda$</sub> , while values above  $2 \text{cm}^2 \text{s}^{-2}$  appear in STRAT <sub>$\lambda$</sub> .

The intensification of EKE in the deep ocean on the eastern flank of MAR visible in Fig. 1c is independent of the currents in the surface layer (i.e., NAC branches). It is generated by the topographically controlled and seasonally variable flow of dense water (Iceland–Scotland Overflow Water; ISOW) that crosses the Iceland–Scotland Ridge, which is better simulated in the experiments with variable eddy transfer coefficient (see, e.g., Fig. 5, described below). This can be readily seen in horizontal EKE sections (not

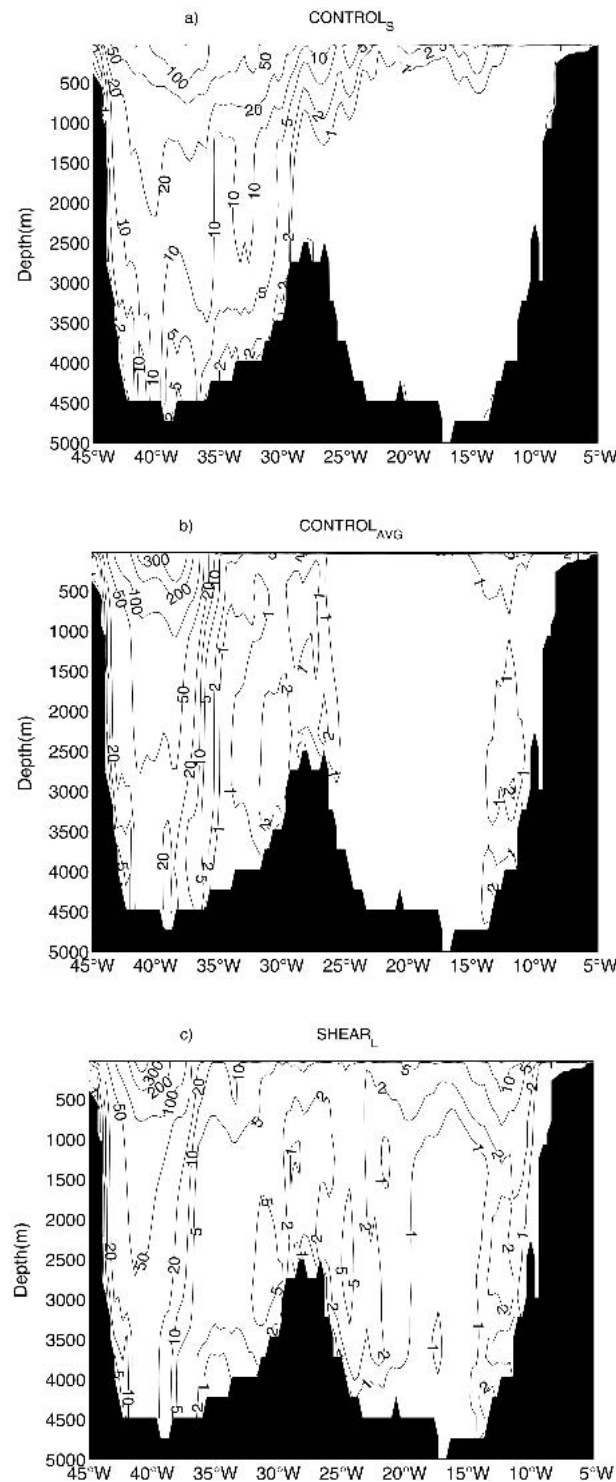


FIG. 1. Eddy kinetic energy ( $\text{cm}^2 \text{s}^{-2}$ ) at  $48^\circ\text{N}$  in (a)  $\text{CONTROL}_S$ , (b)  $\text{CONTROL}_{\text{AVG}}$ , and (c)  $\text{SHEAR}_L$ .

shown) at depths greater than 3000 m, which show widespread eddy variability in the eastern basin, with local maxima around the Rockall Plateau and along the MAR.

## b. Mean circulation

### 1) LABRADOR SEA

The simulated Labrador Current (LC) branches at Hamilton Bank into an offshore branch that flows along the continental slope and an inshore branch that flows over the shelf. Contrary to observations, which indicate higher near-surface velocities for the offshore branch [estimated by Lazier and Wright (1993) to be 2 times those for the inshore branch, near  $54^\circ\text{N}$ ], in  $\text{CONTROL}_S$  the offshore branch of the LC is not only weaker than the inshore branch but also loses its strength as it flows along the slope (Fig. 2a). The relative strength of the LC branches is more realistically reproduced in the other experiments, with a stronger offshore branch all the way to Flemish Cap (Figs. 2b–f). A deep-reaching LC is visible in the vertical sections of the mean meridional velocity at  $53^\circ\text{N}$  shown in Fig. 3. Its almost barotropic structure, with speeds higher than  $15 \text{ cm s}^{-1}$  in all experiments except  $\text{CONTROL}_S$ , are in very good agreement with the observed structure of the deep LC and its average velocity of  $15 \pm 3 \text{ cm s}^{-1}$  at  $54^\circ\text{N}$  estimated by Lazier and Wright (1993), as well as with the mean value of  $18 \text{ cm s}^{-1}$  estimated by Fischer and Schott (2002) for the core speed from float data.

A countercurrent similar to the current opposite and adjacent to the cyclonic boundary currents in the Labrador and Irminger Seas recently revealed by observations (Lavender et al. 2000; Cuny et al. 2002; Fischer and Schott 2002) first occurred in simulations with SPOM when a partial cell approach was used for the bottommost cell (Myers 2002). There are several quasi-stationary cyclonic eddies on the inshore flank of the countercurrent simulated with SPOM, which act as recirculating cells and thus resemble those reported by Lavender et al. (2000). Because the energy analysis performed on the model output by Myers and Deacu (2004) indicated transfer of EKE into KEM in the Labrador Sea region, the authors argued that baroclinic eddies occurring because of baroclinic instability in the frontal region along the Labrador continental slope may be responsible for the acceleration of the countercurrent, producing such a current in the model that is too intense in comparison with the observations.

These eddies may be too energetic in the previous version of the model (i.e., in  $\text{CONTROL}_S$ ), because a high level of available potential energy may need be accumulated in the frontal region before the shedding of an eddy at the scale of the resolved flow is possible. One would expect that an increased release of available potential energy in the region by means of higher values of the bolus velocity would have a positive impact on the simulated countercurrent and circulation in the Labrador Sea. Lower levels of available potential energy have been obtained in  $\text{CONTROL}_{\text{AVG}}$  and in the STRAT and SHEAR experiments, in which the values of the eddy transfer coefficient in the frontal

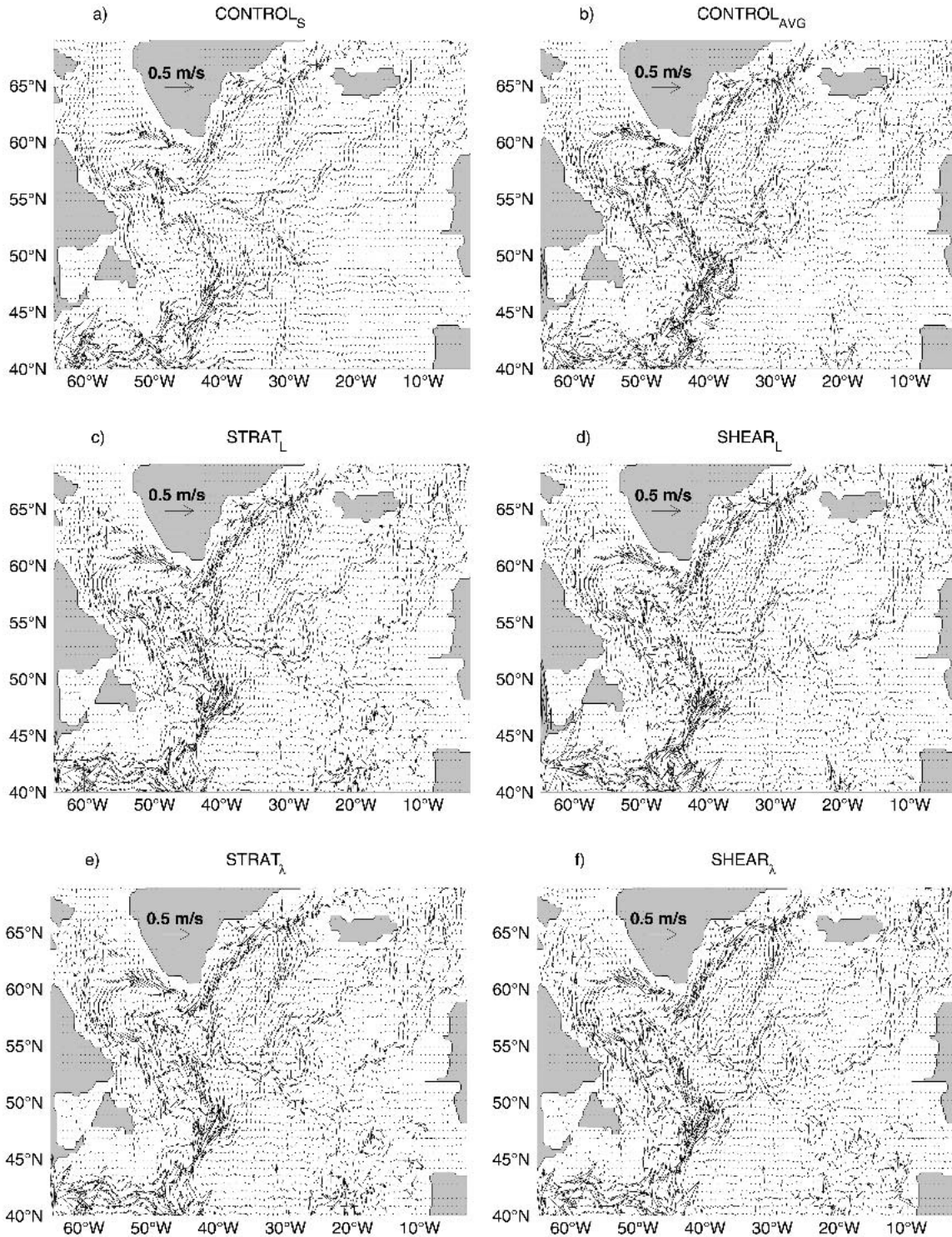


FIG. 2. Time-mean horizontal velocity at 52-m depth in (a) CONTROL<sub>S</sub>, (b) CONTROL<sub>AVG</sub>, (c) STRAT<sub>L</sub>, (d) SHEAR<sub>L</sub>, (e) STRAT<sub>λ</sub>, and (f) SHEAR<sub>λ</sub>. Vectors are plotted at every other grid point.

region are at least one order of magnitude higher than in CONTROL<sub>S</sub>, but this energy level led to a weaker countercurrent in STRAT<sub>L</sub> and SHEAR<sub>L</sub> only (Fig. 3). However, a notable aspect is the reduced strength of

the countercurrent relative to that of the LC in all experiments except CONTROL<sub>S</sub>, which is in better agreement with the pattern obtained from observations (Lavender et al. 2000; Cuny et al. 2002; Fischer and

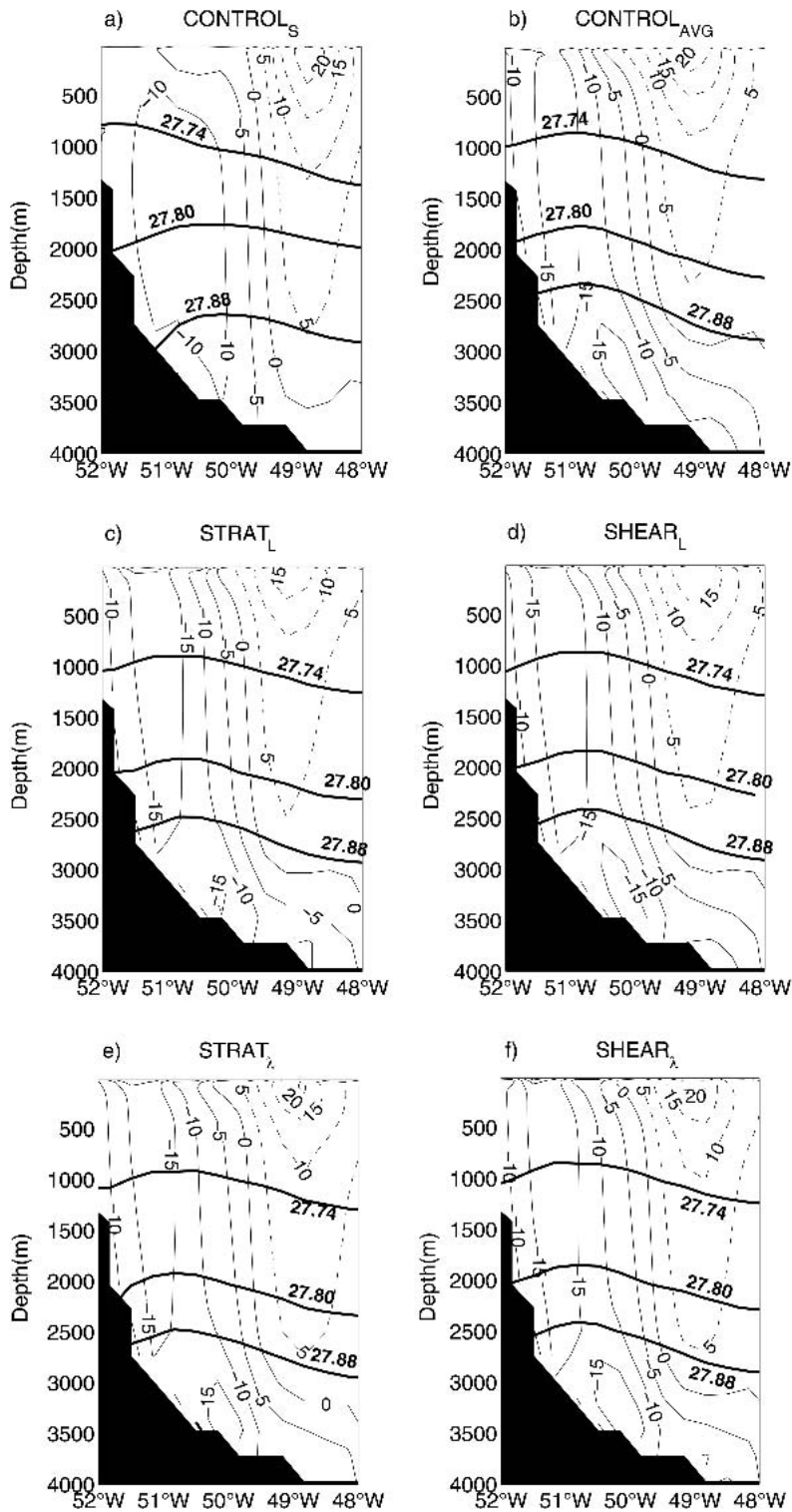


FIG. 3. Cross sections of the mean meridional flow and potential density  $\sigma_0$  at 53°N in (a) CONTROL<sub>S</sub>, (b) CONTROL<sub>AVG</sub>, (c) STRAT<sub>L</sub>, (d) SHEAR<sub>L</sub>, (e) STRAT<sub>λ</sub>, and (f) SHEAR<sub>λ</sub>. The thin continuous and dashed lines are isotachs ( $\text{cm s}^{-1}$ ), and the thick lines depict potential density. Positive and negative values of velocity indicate northward and southward flow, respectively. The 27.74 and 27.80 isopycnals are the limits for the Labrador Sea Water. The ISOW layer is limited by the 27.80 and 27.88 isopycnals and overlies the DSOW layer.

Schott 2002). Velocities between 5 and 10  $\text{cm s}^{-1}$  have been obtained for the countercurrent in the Labrador Sea Water (LSW) layer, at 53°N in all experiments (Fig. 3), and these values are close to the ones measured by Fischer and Schott (2002).

A distinct feature visible in the experiments with reduced horizontal diffusion is the deep core of the deep western boundary current (DWBC), whose axis lies above the 3500-m isobath at 53°N (Figs. 3b–f). Its location and velocity values ( $>15 \text{ cm s}^{-1}$ ) at this latitude are consistent with those indicated by Fischer and Schott (2002) (see their Fig. 4b). The current is indistinguishable from the deep Labrador Current in CONTROL<sub>S</sub> (Fig. 3a). The DWBC is a major component of the large-scale meridional overturning circulation. Its realistic simulation, crucial for coupled climate modeling, requires accurate representation of the overflow waters that form the North Atlantic Deep Water carried by this current (Willebrand et al. 2001). Eddy-permitting  $z$ -level ocean models have difficulties in this respect, and bottom boundary layer schemes (Beckmann and Döscher 1997) have been devised to address this issue. An explanation of the improved simulation of the DWBC in our experiments with reduced horizontal diffusion is given in section 4c.

## 2) THE NORTH ATLANTIC CURRENT AND EASTERN BASIN

The mean near-surface current pattern obtained in all experiments (Fig. 2) shows the NAC as a relatively narrow current east of the Grand Banks (approximately 45°N and 43°W), which branches near 46°N. There is a branch that flows northeastward and then crosses the Mid-Atlantic Ridge, which is visibly wider in CONTROL<sub>S</sub>, most likely because of increased eddy activity in the region in this experiment. In the other experiments, this branch stays closer to the inshore branch before turning northeastward at about 50°N.

A narrower but strong branch flows past Flemish Cap and then northwestward into the Labrador Sea. The latter fails to follow its classical path with an eastward turning in the region known as the “Northwest Corner” at 52°N (Krauss 1986; Lavender et al. 2000). Instead, it continues into the Labrador Sea, associated with the countercurrent discussed above. The countercurrent is still too intense in all of the experiments, and this error has a major negative impact on the strength and pathway of the simulated NAC, by entraining much of its water into the Labrador Sea and thus affecting the eastward shift of the NAC at the Northwest Corner.

One of the remarkable differences in the near-surface circulation in the eastern basin consists in the flow pattern around the Reykjanes ridge. An anticyclonic flow around the ridge is obtained in CONTROL<sub>S</sub>, whose southwestward component on the eastern flank originates from the NAC branch in the Iceland Basin (Fig. 2a). In the experiments with reduced horizontal

diffusion, this component is very weak relative to the intense northeastward current on the western flank of the ridge (the Irminger Current) and the branch of the NAC flowing in the Iceland basin (Figs. 2b–f). This result is in better agreement with the pattern of the average surface circulation derived from drifter data by Flatau et al. (2003). In none of the experiments, however, does the Irminger Current show up as a branch of the NAC as in Flatau et al. (2003). The presence of the relatively strong southwestward current in CONTROL<sub>S</sub> leads a higher entrainment and recirculation of NAC water in the subpolar gyre, whereas most of this water appears to be carried across the Iceland–Scotland Ridge into the Norwegian Basin in the other experiments.

Another interesting feature of the upper-layer circulation in the eastern basin is the branch of NAC that flows around the Rockall Plateau into the Rockall Trough, which follows more closely the topography in the experiments with reduced horizontal diffusion. Observational data support the association of this branch with the local topography (Flatau et al. 2003). The current appears to be strongly influenced by the flow of the model’s ISOW through the Rockall Trough. The steepening of the isopycnals occurring as this water flows against the southeastern slope of the Rockall Plateau may lead to the generation of this current as a quasi-geostrophic current, which thus bears some resemblance to the countercurrent in the Labrador Sea.

### c. Overflow waters

The steplike topography of the  $z$ -level ocean models induces significant spurious vertical mixing of the overflow waters during their downslope spreading (Beckmann and Döscher 1997). The use of partially filled bottom cells reduces this unwanted effect and enhances the propagation of the overflow plume by reducing the height of the step between adjacent bottommost cells (Kåse et al. 2001). On the other hand, Ezer and Mellor (2004) have shown that this spurious vertical mixing intensifies with increased horizontal diffusion in  $z$  models and concluded that the replacement of the horizontal diffusion with an isopycnal diffusion scheme might lead to an improved simulation of the downslope spreading of the overflow waters. Results from our experiments that employ the GM scheme and have a low background horizontal diffusion support this conclusion. Thus, the more stratified and clearly identifiable DWBC obtained in these experiments is nothing else but the product of a better representation of the model’s overflow waters [Denmark Strait Overflow Water (DSOW) and ISOW] consisting in an improved capability to maintain their watermass properties as they flow against the Greenland and Labrador continental slopes (Fig. 4).

Figure 3 shows that the 27.80 isopycnal that caps the overflow water mass in our model remains at about the same depth along the Labrador slope in all experi-

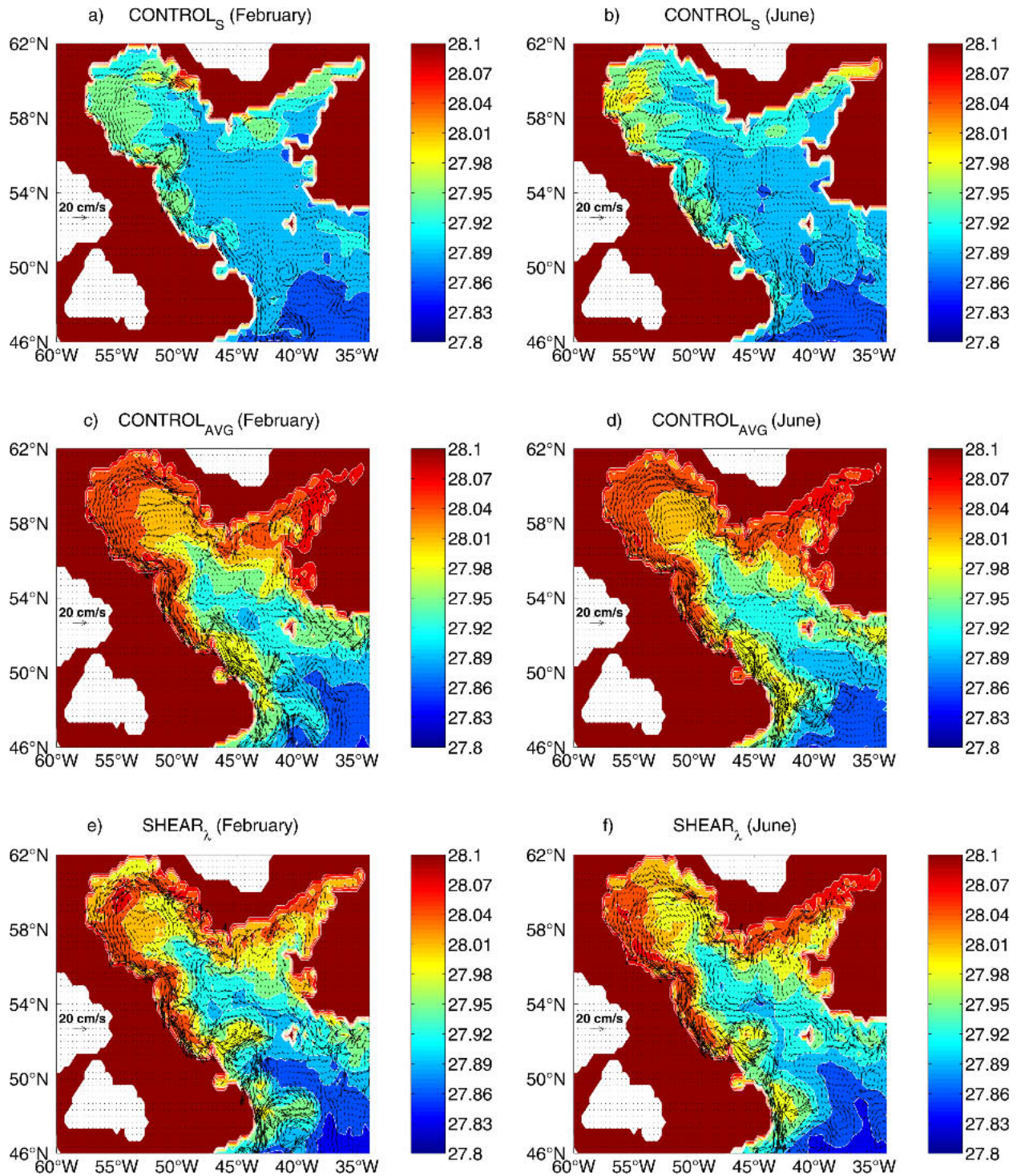


FIG. 4. Potential density ( $\sigma_0$ ) at 3225-m depth for model days 4920 (in Feb, year 14) and 5040 (in Jun, year 14) in (a),(b) CONTROL<sub>S</sub>, (c),(d) CONTROL<sub>AVG</sub>, and (e),(f) SHEAR <sub>$\lambda$</sub> . The contour interval is 0.03. Superimposed are the horizontal velocity vectors at the same depth and time.

ments. However, the ISOW layer (bounded by the 27.80 and 27.88 isopycnals) is thicker in CONTROL<sub>S</sub> (Fig. 3a) than in the other experiments (Figs. 3b–f), whereas the DSOW layer (beneath the 27.88 isopycnal)

is thinner. The continuous transformation of the water-mass properties of the DSOW along its path through spurious mixing with ambient water is considered to be a principal mechanism whereby this water becomes

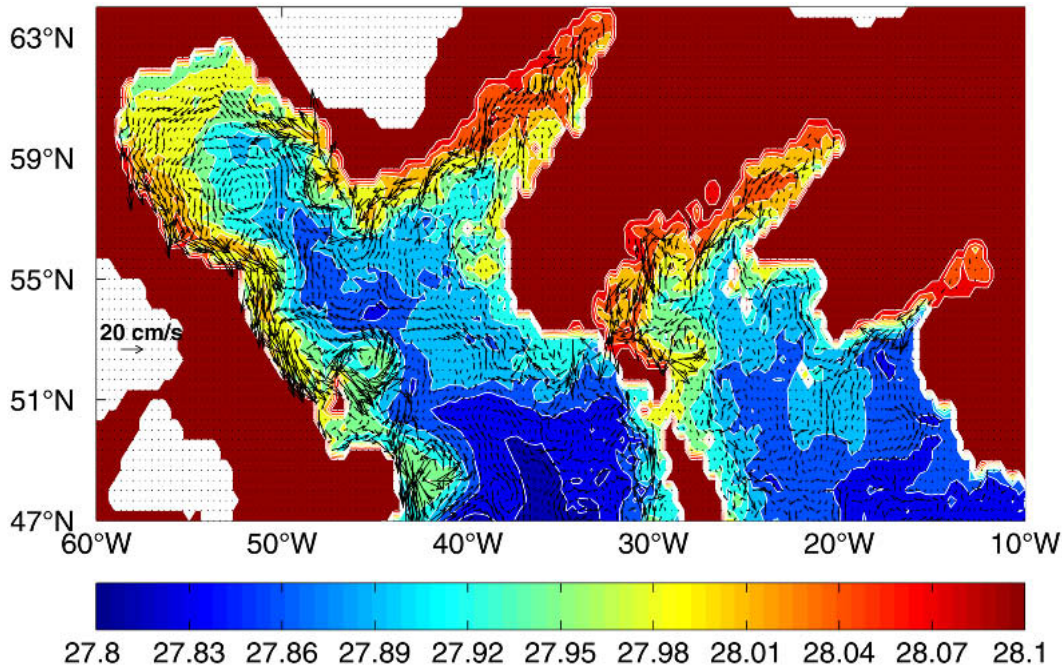


FIG. 5. Potential density ( $\sigma_0$ ) at 2980-m depth for model day 5040 (in Jun, year 14) in SHEAR $_{\lambda}$ . The contour interval is 0.03. Superimposed are the horizontal velocity vectors at the same depth and time.

lighter and thus contributes to the thickness of the ISOW layer in CONTROL $_S$ . This mechanism also explains why the density-driven DWBC is weaker and hardly distinguishable from the deep LC in the same experiment. A very similar situation has been reported by Ezer and Mellor (2004) for an idealized case in which a thicker intermediate water mass resulted from a decreased downslope spreading of their dense plume combined with enhanced spurious mixing of the dense water with ambient water as the horizontal diffusion was increased in their experiments with a  $z$ -level model.

Another aspect that fits in this context is that of the link between the numerical stability of SPOM and the representation of the overflow waters. It is very likely that the reduced vertical mixing due to convective adjustment triggered by statically unstable regions at the bottom, which occurs when dense water overlies lighter water, may have had a positive impact on the numerical stability. This effect, first noticed and reported by Mellor et al. (2002) and Ezer and Mellor (2004), may partly explain why SPOM remained numerically stable despite the significant reduction in horizontal diffusion.

The two quasi-stationary cyclonic eddies visible at all levels near 52° and 56°N (offshore of the Labrador continental slope) have a major impact on the circulation simulated with SPOM in all experiments by controlling the intensity of the countercurrent (Figs. 2 and 4). They initially were thought to be generated entirely through baroclinic instability in the frontal region. Therefore, they were expected to become less energetic as a result of increased release of available potential energy in ex-

periments that used higher values for eddy transfer coefficient in the region, and this was one of the motivations of the study presented herein. However, the expected behavior seems to have occurred to some extent in STRAT $_L$  and SHEAR $_L$  only. Further investigation took into consideration the DWBC and revealed that its interaction with topography is associated with the above-mentioned eddies. Thus, the eddy near 56°N appears to be related to the doming of isopycnals produced by the accumulation of dense water where the DWBC abruptly changes its direction, northeast of Hamilton Bank (Fig. 4). The other eddy is generated where the DWBC is deflected seaward by the Orphan Knoll (Figs. 4 and 5); similar cyclonic circulation in this region has been identified observationally (Fischer and Schott 2002; Lavender et al. 2000). There are also transient eddies that occur along the pathway of the DWBC (along the Labrador continental slope and offshore Flemish Cap) in all experiments (Fig. 4), but only an in-depth investigation can tell us whether they are due to shear instability or to baroclinic instability.

A remarkable improvement relative to CONTROL $_S$  is the simulation of the flow of dense water (ISOW) originating from the Norwegian Sea in all of the other experiments. Most of this water flows along the eastern slope of the Reykjanes Ridge, and then part of it flows around the ridge to enter the Irminger Basin while the rest continues its path along the eastern flank of MAR. Figure 5 shows the interaction of this flow with a topographic feature near 52°N and 31°W, which is a coarse representation of the Recate Seamount in the model on

the south side of the Charlie Gibbs Fracture Zone. The density-driven current is deflected by this feature, and a cyclonic recirculation centered near 52.5°N and 28°W (Figs. 2b–f) occurs. The quasi-stationary eddy generated here resembles that identified from observations by Bower et al. (2002), although it is located about 2° east of this one. Notice, however, that the location of the simulated eddy is sensitive to the grid resolution as well as to the representation of the topography. There is also flow of ISOW along the southeastern and southwestern slopes of the Rockall Plateau.

As mentioned previously, the improved representation of the dense overflow waters (DSOW and ISOW) in the model, in the experiments with reduced horizontal diffusion, has led to the simulation of a stronger and more clearly identifiable DWBC. As a consequence, one would expect an increased southward transport of the meridional overturning circulation (MOC). Figure 6 depicts the meridional overturning streamfunction calculated from the mean meridional velocity field averaged over the last four years of the integration. In both CONTROL<sub>AVG</sub> and SHEAR<sub>λ</sub>, the overturning circulation is stronger than in CONTROL<sub>S</sub>. The overturning transport at 40°N is 19 Sv (1 Sv ≡ 10<sup>6</sup> m<sup>3</sup> s<sup>-1</sup>) in CONTROL<sub>S</sub>, 41 Sv in CONTROL<sub>AVG</sub>, and 32 Sv in SHEAR<sub>λ</sub> (the values for all of the experiments are given in Table 2). The strength of the meridional overturning circulation in the North Atlantic obtained in CONTROL<sub>S</sub> is in better agreement with the observational estimates, which are less than 20 Sv (Ganachaud and Wunsch 2000). The unrealistically high values obtained in the rest of the experiments are the result of the generally larger mean meridional velocities used in calculations. The latter are not brought about by an unreasonably high production and transport of North Atlantic Deep Water (LSW, ISOW, and DSOW), but rather by the occurrence of more energetic mean flows due to reduced velocity shear in those experiments.

Note that, in all of the experiments with reduced horizontal diffusion, the returning southward component of meridional overturning circulation is more concentrated toward the bottom (Fig. 6). This downward shift is somewhat similar to that obtained by Dengg et al. (1999), when a BBL scheme was used to facilitate the flow of the dense waters in an eddy-permitting model of the subpolar North Atlantic while preserving its properties. However, the overturning transport exhibited changes of only 1 Sv in their experiments. Significant sensitivity of the Atlantic MOC to the overflow waters originating from the Nordic seas was found in modeling studies carried out by Döscher et al. (1994) and Döscher and Redler (1997).

*d. Salinity*

To assess the effect of the variable eddy transfer coefficients on the freshwater content of the Labrador Sea, this quantity has been calculated for the Labrador Sea region between latitudes 52° and 64°N (shown in

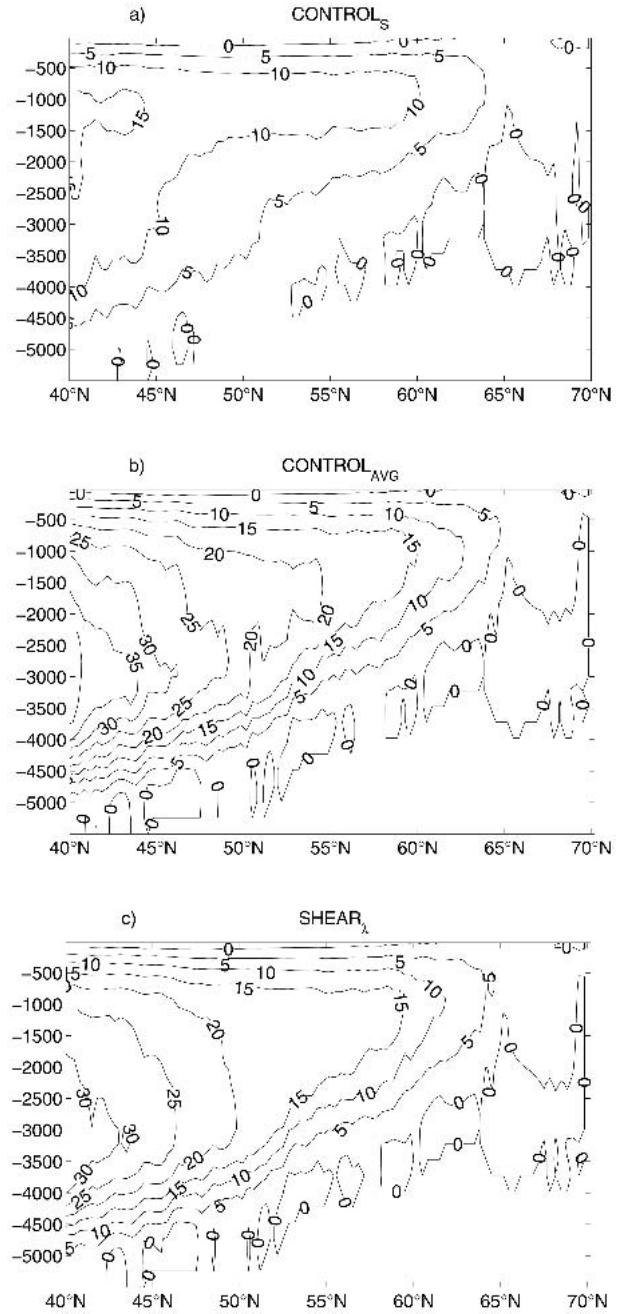


FIG. 6. Meridional overturning streamfunction for the subpolar North Atlantic (Sv) in (a) CONTROL<sub>S</sub>, (b) CONTROL<sub>AVG</sub>, and (c) SHEAR<sub>λ</sub>. The contour interval is 5 Sv.

Fig. 7) every 3 months and through the entire period of integration. The formula used for freshwater content is

$$FW = \int_V \frac{S_r - S}{S_r} dV, \quad (11)$$

where  $V$  is the volume of the domain under consideration,  $S$  is the model output salinity, and  $S_r$  is a refer-

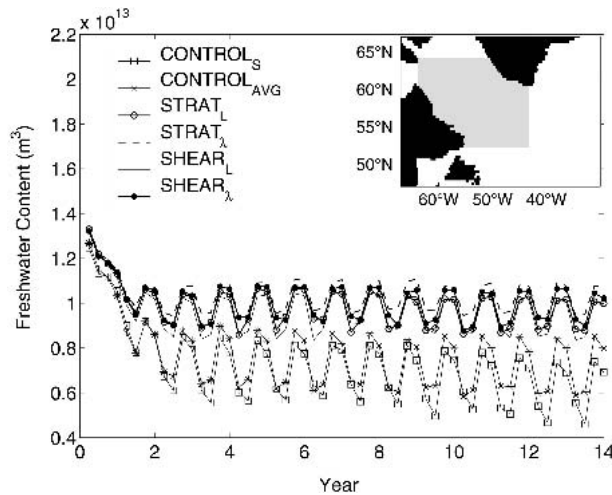


FIG. 7. Freshwater content for a limited region in the Labrador Sea (the gray-shaded region in the upper-right corner of the figure).

ence salinity [with a value of 35.0 psu, chosen to be consistent with the model salinity in  $\text{CONTROL}_S$  at the offshore edge of the Labrador Current; see Myers (2002) for more details]. Figure 7 shows that there are no major differences in the freshwater content time series obtained in the experiments with variable eddy transfer coefficients. They all have seasonal variations characterized by smaller amplitudes and higher annual mean values relative to the two  $\text{CONTROL}$  experiments. An improvement in these simulations consists in the diminished loss of freshwater indicated by the higher annual mean values obtained after the initial drift from the initial conditions has ceased. This instance is one of the few in which a clear distinction can be made between the results obtained from the experiments with variable eddy transfer coefficients and  $\text{CONTROL}_{\text{AVG}}$ , and it shows that small local differences can lead to dissimilar global effects. A seasonal equilibrium has also been reached in all experiments other than  $\text{CONTROL}_S$ .

Although the 14-yr period of integration is insufficient for the model to reach a thermodynamical equilibrium, some qualitative comparisons involving the salinity fields evolved from the initial conditions can be made. The time-mean salinity has been plotted on the  $\sigma_2 = 36.95$  isopycnal surface, which is representative for the LSW, to offer a qualitative view of the spreading of this water in three different experiments (Fig. 8). Salinity is overpredicted in the Labrador Sea in all experiments, because the observed salinity values associated with the LSW are typically less than 34.9 psu (Lilly et al. 1999). This is a typical problem in non-eddy-resolving models of the North Atlantic. A reduction in salinities in the Labrador and Irminger basins is obtained in  $\text{CONTROL}_{\text{AVG}}$  (Fig. 8b). Further reductions occur in the experiments with variable eddy transfer coefficients

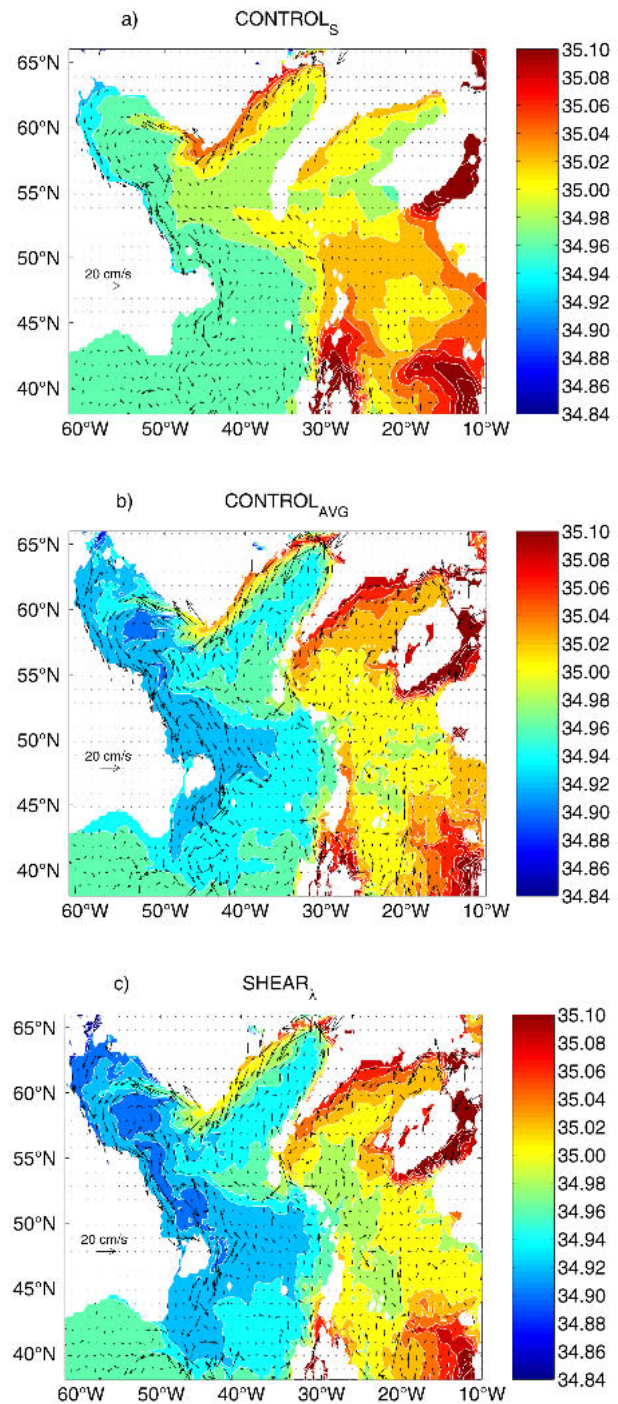


FIG. 8. Time-mean salinity (psu) on the  $\sigma_2 = 36.95$  isopycnal in (a)  $\text{CONTROL}_S$ , (b)  $\text{CONTROL}_{\text{AVG}}$ , and (c)  $\text{SHEAR}_A$ . The contour interval is 0.02. Superimposed are vectors of the mean horizontal velocity (plotted at every other grid point) on the same isopycnal surface.

(Fig. 8c), which are the closest to the observations. These changes on this isopycnal surface are brought about by a shift in LSW formation from saltier to fresher water classes.

The LSW on the  $\sigma_2 = 36.95$  isopycnal is associated with a minimum in salinity (Fig. 8). The plots obtained in  $\text{CONTROL}_{\text{AVG}}$  and  $\text{SHEAR}_\lambda$  (Figs. 8b,c) illustrate two main pathways of spreading of the LSW from the deep convection region (centered at about  $58^\circ\text{N}$  and  $53^\circ\text{W}$  in the model). One pathway is established through the spreading of LSW from the deep convection region toward the LC, followed by embedment in the LC and southward transport by this current, along with spreading toward the eastern North Atlantic basin along the pathway of the NAC. Notice that the MAR acts as a barrier to the spreading of the LSW into the eastern basin along this isopycnal because of its high depth in the model. The other pathway is from the deep convection region to the Irminger Sea. It occurs as a result of entrainment of LSW into the countercurrent simulated in the Labrador Sea, which reaches into the Irminger Sea. Of interest is that part of the water following this path is LSW recirculated by the countercurrent along the Labrador slope.

Salinity sections at  $53^\circ\text{N}$  (Fig. 9) show that an improved representation of the LSW (visible as the tongue of relatively homogeneous low-salinity water centered at 2000-m depth in Figs. 9b,c) and its seaward spreading is obtained in  $\text{CONTROL}_{\text{AVG}}$  and  $\text{SHEAR}_\lambda$ . Similar results have been obtained in the other experiments with variable eddy transfer coefficients. Consistent with the freshwater content analysis (Fig. 7), the LSW core salinity is lower in  $\text{SHEAR}_\lambda$ .

#### e. GM velocities

Instantaneous horizontal bolus velocity fields obtained in the  $\text{SHEAR}_L$  experiment have been plotted every 30 days over the period February–July of the last year of integration, on level 20 of the model ( $\sim 1500\text{-m}$  depth). These fields are depicted in Fig. 10. The plot for model day 4920 (February) shows that high magnitudes for this quantity are concentrated in the region of the Labrador Sea where the simulated deep convection occurs at this time of the year and along the northeastern part of the east Greenland slope, on the path of the DSOW. The bolus velocity in the deep convection region induces an outflow at depths between approximately 700 and 2300 m that carries LSW toward the shore, where it gets embedded into the southward-flowing boundary currents, and toward the countercurrent leading to direct LSW export to the Irminger Sea (Figs. 10b,c). This flow is matched by an inflow at shallower depths, advecting lighter water toward the interior of the gyre. This circulation is similar to the eddy-induced “overturning circulation” in the deep convection region of the Labrador Sea proposed by Khatiwala and Visbeck (2000). The plots of the eddy-induced velocity for the next three months indicate a postconvection spreading toward the boundary, which is associated with slumping of steep isopycnals. This process leads to a large decrease in baroclinic activity in the region as a consequence of the restratification of the

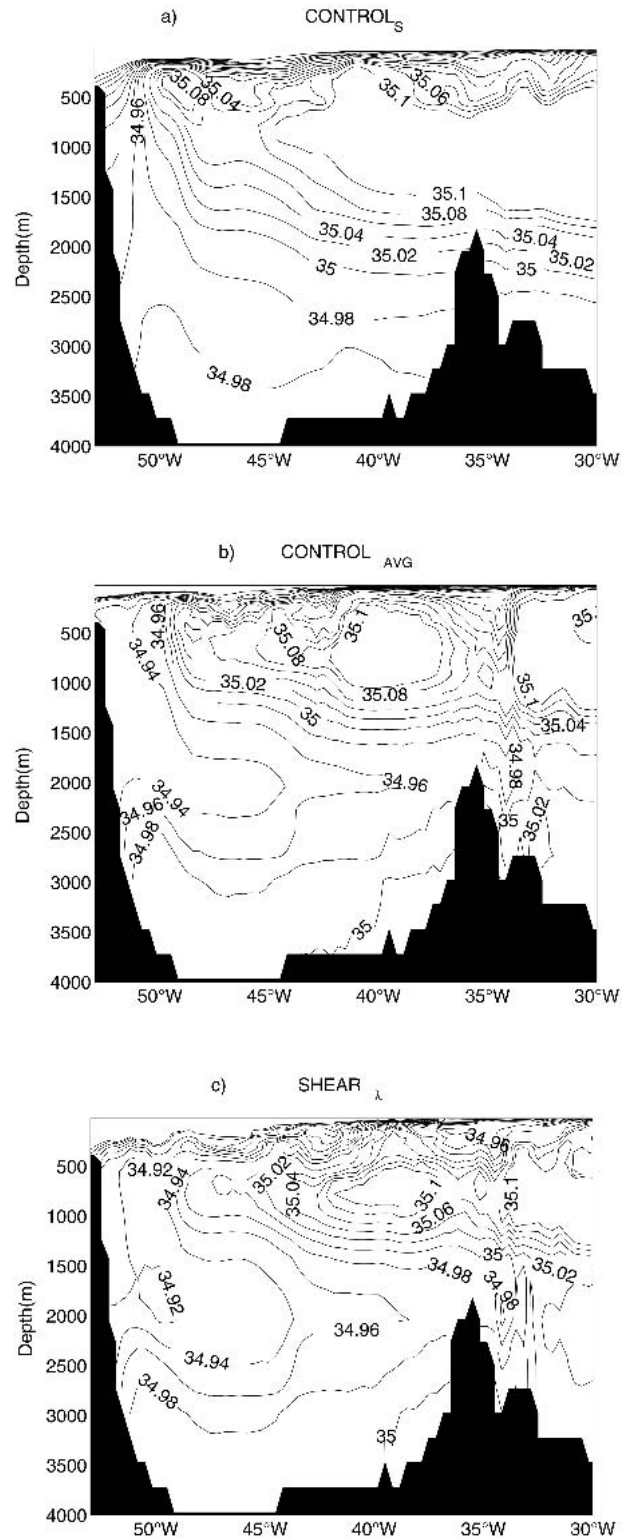


FIG. 9. Time-mean salinity (psu) at  $53^\circ\text{N}$  in (a)  $\text{CONTROL}_S$ , (b)  $\text{CONTROL}_{\text{AVG}}$ , and (c)  $\text{SHEAR}_\lambda$ . The tongue of low salinity centered at 2000-m depth, which is visible on the right-hand side of (b) and (c), corresponds to the model's Labrador Sea Water. Only contours for salinity values between 34.8 and 35.1 psu have been plotted. The contour interval is 0.02.

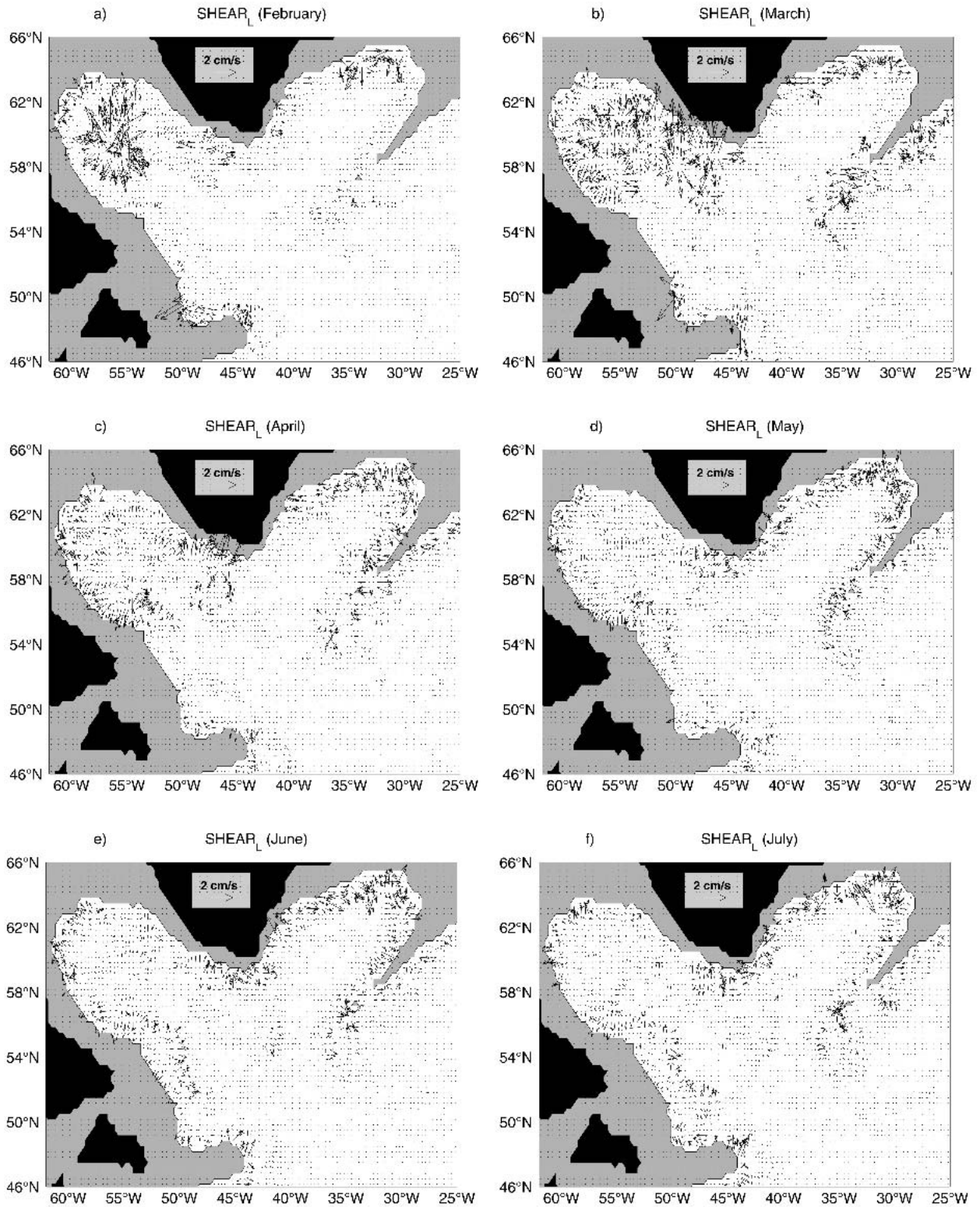


FIG. 10. The GM/bolus/eddy-induced velocity vector fields obtained in the SHEAR<sub>L</sub> experiment on level 20 (~1500 m) for the model days (a) 4920 (Feb), (b) 4950 (Mar), (c) 4980 (Apr), (d) 5010 (May), (e) 5040 (Jun), and (f) 5070 (Jul) of the 14th year of integration from rest.

water mass. An eddy-induced flow is visible in the frontal region of the Labrador Current in the plots for June and July. The steepening of the isopycnals that occurs as the Labrador Current is transporting LSW southward leads to the intensification of the eddy-induced flow. This suggests a timescale of 4–5 months for the LSW to reach Flemish Cap from the deep convection region. Plots of the potential density (not shown) on level 15 show that the LSW spreading toward the LC followed by its southward transport is simulated in the experiments with reduced horizontal diffusion only. Notice also the intensification in time of the eddy-induced flow along the east Greenland slope as well as on the western side of the Reykjanes Ridge. This flow is generated by the steepening of isopycnals caused by the seasonally variable flow of ISOW and DSOW at depth.

## 5. Conclusions

A variable eddy transfer coefficient for the GM parameterization has been tested in a  $(1/3)^\circ$ -resolution ocean model of the subpolar North Atlantic. The aim of the study is to assess the impact of the quasi-adiabatic transport/stirring of tracers by means of eddy-induced velocities that use either variable or constant eddy transfer coefficients and a low level of explicit horizontal diffusion, in the eddy-permitting regime.

Two formulas have been employed for the computation of the eddy transfer coefficient field, each of them implemented in two different ways. Results from the four experiments corresponding to the four formula-implementation pairs have been compared with results from two control experiments. In both control experiments, the eddy-induced velocities are calculated using a constant eddy transfer coefficient. The one that uses a lower value for this coefficient also uses a typical value of the biharmonic horizontal diffusion coefficient for the eddy-permitting regime. The second control experiment employs a larger eddy transfer coefficient and a significantly lower horizontal diffusion coefficient.

More realistic and very similar simulations have been obtained in all of the experiments with a low level of horizontal diffusion—that is, in the experiments with variable eddy transfer coefficients and in the control experiment with a higher value of this coefficient. Therefore, we conclude that the reduction of the spurious diapycnal mixing obtained in these experiments has a primary positive impact on the circulation and hydrography, whereas the use of a variable eddy transfer coefficient has secondary importance. Nonetheless, aside from its physically motivated use, there are instances of better predictions for global quantities (e.g., overturning transport or freshwater content of the Labrador Sea) that indicate that a variable eddy transfer coefficient is preferable.

Many of the improvements obtained in the experi-

ments with reduced horizontal diffusion are brought about by a better representation of the overflow waters originating from the Nordic seas. Among these are a more realistic deep western boundary current and increased eddy activity in the deep ocean in the eastern North Atlantic. In the same experiments, the higher values of the GM velocities combined with a reduced spurious diapycnal mixing in the deep convection region at the time that the deep convection is occurring “help” the Labrador Sea Water to spread from this region to the currents that surround it. Two classical pathways for the spreading of this water, one via the Labrador Current and the other via the countercurrent in the Labrador Sea, are then established.

The relative strength of the two branches of the Labrador Current and the almost barotropic structure of its offshore branch as well as the near-surface circulation in the eastern North Atlantic simulated in the experiments with low horizontal diffusion are in better agreement with flow patterns inferred from observations. A flow that is more energetic but less time variable is obtained in the same experiments. The undesirable effect of reduced eddy activity in the upper layers is the result of the increased release of available potential energy.

A strong countercurrent occurs in the Labrador Sea, in all of the experiments. This current has a negative impact on the pathway of the NAC in the Northwest Corner and on the hydrography of the Labrador Sea by entraining NAC water into the region. However, in the experiments with variable eddy transfer coefficients, the existence of a larger volume of LSW along the Labrador slope leads to an increased recirculation of this water mass and thus diminishes the model salinity drift in the Labrador Sea.

Because very similar results have been obtained in all of the experiments with variable eddy transfer coefficients, none of the four formula-implementation pairs used for this coefficient stands out as the best. Note, however, that the eddy coefficient field was found to be more “dynamic” in the SHEAR experiments than in the STRAT experiments, in the sense that it changed more rapidly in time. Moreover, the same field had a smaller time- and domain-average value and led to higher EKE/KEM ratios, indicating increased variability of the flow. Tuning of the constants used in the expressions for the eddy transfer coefficient has not been tested, but it can provide a means of limiting the possible overparameterization of the effect of mesoscale eddies when using eddy-induced velocities with variable eddy transfer coefficients in eddy-permitting ocean models.

*Acknowledgments.* We thank Peter Gent, Richard Greatbatch, and two anonymous reviewers for their helpful comments. This work is part of the Ph.D. research work of Daniel Deacu and was funded by NSERC and CFCAS grants awarded to Paul G. Myers.

## APPENDIX

## Details of the Length-Scale Algorithm

The algorithm for determining the length scale entering the expression of the variable eddy transfer coefficient (2) is attributed to the Hadley Centre and is described in more detail in the MOM3 manual (Pacanowski and Griffies 1998). In our model, this length scale is calculated separately at “ugent” and “vgent” velocity points on a C grid, using the same algorithm, and an upper limit is imposed on its value. At a given ugent velocity grid point, the algorithm starts by setting the length scale equal to  $\Delta y$  (the meridional grid spacing), which is also  $\max(\Delta x, \Delta y)$ . If the growth rate at this point is less than a threshold value of  $1.4 \times 10^{-6} \text{ s}^{-1}$  (Wright 1997), which is equivalent to a time scale greater than 8.25 days, then the length scale remains unchanged. Otherwise it is considered that the grid point may belong to a larger baroclinic region. In the latter case, a search is performed in the four directions of the neighboring ugent grid points to determine the extent of this region. The search is stopped when a node with a growth rate smaller than the threshold value is encountered. Such a node is considered to be outside the baroclinic region, and the distance to it is evaluated. The length scale corresponding to the given grid point will then be calculated from the four distances thus determined. Because we want to avoid the parameterization of the effects of the resolved eddies, we consider limiting the search to the first node in each of the four directions as acceptable. In the limiting case in which all four neighboring ugent grid points are found to belong to the baroclinic region associated with the given ugent grid point, the algorithm returns a maximum value of  $3\Delta x = \min(3\Delta x, 3\Delta y)$  for the length scale, which corresponds to  $1^\circ$  of latitude in our model. Note that this value is smaller than the upper bound  $3\Delta y$  ( $1^\circ$  of longitude) imposed on the unresolved baroclinic eddies in the model. Notice also that the square of the maximum length scale will be almost one order of magnitude larger than the square of the minimum value, at the same latitude. As a consequence, the maximum value of the eddy transfer coefficient will differ by roughly one order of magnitude from its minimum value for the same value of the growth rate.

## REFERENCES

- Adcroft, A., C. Hill, and J. Marshall, 1997: Representation of topography by shaved cells in a height coordinate ocean model. *Mon. Wea. Rev.*, **125**, 2293–2315.
- Beckmann, A., and R. Döscher, 1997: A method for improved representation of dense water spreading over topography in geopotential-coordinate models. *J. Phys. Oceanogr.*, **27**, 581–591.
- Beismann, J. O., and R. Redler, 2003: Model simulations of CFC uptake in North Atlantic Deep Water: Effects of parameterizations and grid resolution. *J. Geophys. Res.*, **108**, 3159, doi:10.1029/2001JC0011253.
- Böning, C. W., R. Holland, F. Bryan, G. Danabasoglu, and J. C. McWilliams, 1995: An overlooked problem in model simulations of the thermohaline circulation and heat transport in the Atlantic Ocean. *J. Climate*, **8**, 515–523.
- Bower, A. S., and Coauthors, 2002: Directly measured mid-depth circulation in the northeastern North Atlantic Ocean. *Nature*, **419**, 603–607.
- Bryan, K., J. K. Dukowicz, and R. D. Smith, 1999: On the mixing coefficient in the parameterization of bolus velocity. *J. Phys. Oceanogr.*, **29**, 2442–2456.
- Colin de Verdière, A., H. Mercier, and M. Arhan, 1989: Mesoscale variability from the western to the eastern Atlantic along  $48^\circ\text{N}$ . *J. Phys. Oceanogr.*, **19**, 1149–1170.
- Cox, M. D., 1987: Isopycnal diffusion in a  $z$ -coordinate ocean model. *Ocean Modelling*, **74** (unpublished manuscripts), 1–5.
- Cuny, J., P. B. Rhines, P. P. Niiler, and S. Bacon, 2002: Labrador Sea boundary currents and the fate of the Irminger Sea Water. *J. Phys. Oceanogr.*, **32**, 627–647.
- Danabasoglu, G., and J. C. McWilliams, 1995: Sensitivity of the global ocean circulation to parameterizations of mesoscale tracer transports. *J. Climate*, **8**, 2967–2987.
- , —, and P. R. Gent, 1994: The role of mesoscale tracer transports in the global ocean circulation. *Science*, **264**, 1123–1126.
- Dengg, J., C. Böning, U. Ernst, R. Redler, and A. Beckmann, 1999: Effects of an improved model representation of overflow water on the subpolar North Atlantic. *International WOCE Newsletter*, No. 37, WOCE International Project Office, Southampton, United Kingdom, 10–14.
- Döscher, R., and R. Redler, 1997: The relative importance of northern overflow and subpolar deep convection for the North Atlantic thermohaline circulation. *J. Phys. Oceanogr.*, **27**, 1894–1902.
- , C. W. Böning, and P. Herrmann, 1994: Response of circulation and heat transport in the North Atlantic to changes in thermohaline forcing in northern latitudes: A model study. *J. Phys. Oceanogr.*, **24**, 2306–2320.
- England, M. H., and G. Holloway, 1998: Simulations of CFC content and water mass age in the deep North Atlantic. *J. Geophys. Res.*, **103**, 15 885–15 901.
- Ezer, T., and G. L. Mellor, 2004: A generalized coordinate ocean model and a comparison of the bottom boundary layer dynamics in terrain-following and in  $z$ -level grids. *Ocean Modelling*, **6**, 379–403.
- Fischer, J., and F. A. Schott, 2002: Labrador Sea Water tracked by profiling floats—From the boundary current into the open North Atlantic. *J. Phys. Oceanogr.*, **32**, 573–584.
- Flatau, M. K., L. Talley, and P. P. Niiler, 2003: The North Atlantic Oscillation, surface current velocities, and SST changes in the subpolar North Atlantic. *J. Climate*, **16**, 2355–2369.
- Ganachaud, A., and C. Wunsch, 2000: Improved estimates of global ocean circulation, heat transport and mixing from hydrographic data. *Nature*, **408**, 453–456.
- Gent, P. R., and J. C. McWilliams, 1990: Isopycnal mixing in ocean circulation models. *J. Phys. Oceanogr.*, **20**, 150–155.
- , J. Willebrand, T. McDougall, and J. C. McWilliams, 1995: Parameterizing eddy-induced tracer transports in ocean circulation models. *J. Phys. Oceanogr.*, **25**, 463–474.
- , F. Bryan, S. Doney, and W. Large, 1999: A perspective on the ocean component of climate models. *Exchanges*, **14**, 11–14.
- , A. P. Craig, C. M. Bitz, and J. W. Weatherly, 2002: Parameterization improvements in an eddy-permitting ocean model for climate. *J. Climate*, **15**, 1447–1459.
- Gerdes, R., C. Koberle, and J. Willebrand, 1991: The influence of numerical advection schemes on the results of ocean general circulation models. *Climate Dyn.*, **5**, 211–226.
- Grey, S. M., and K. Haines, 1999: Climatological hydrography of the North Atlantic. *International WOCE Newsletter*, No. 36,

- WOCE International Project Office, Southampton, United Kingdom, 23–25.
- Haines, K., and P. Wu, 1998: GCM studies of intermediate and deep waters in the Mediterranean. *J. Mar. Syst.*, **18**, 197–214.
- Held, I. M., and V. D. Larichev, 1996: A scaling theory for horizontally homogeneous, baroclinically unstable flow on a beta plane. *J. Atmos. Sci.*, **53**, 946–952.
- Käse, R. H., A. Biastoch, and D. B. Stammer, 2001: On the mid-depth circulation in the Labrador and Irminger Seas. *Geophys. Res. Lett.*, **28**, 3433–3436.
- Khatiwala, S., and M. Visbeck, 2000: An estimate of the eddy-induced circulation in the Labrador Sea. *Geophys. Res. Lett.*, **27**, 2277–2280.
- Killworth, P. D., D. Staniforth, D. J. Webb, and S. M. Patterson, 1991: The development of a free-surface Bryan–Cox–Semtner ocean model. *J. Phys. Oceanogr.*, **21**, 1333–1348.
- Krauss, W., 1986: The North Atlantic Current. *J. Geophys. Res.*, **91**, 5061–5074.
- Lavender, K. L., R. E. Davis, and W. B. Owens, 2000: Mid-depth recirculation observed in the interior Labrador and Irminger Seas by direct velocity measurement. *Nature*, **407**, 66–69.
- Lazier, J. R. N., and D. G. Wright, 1993: Annual velocity variations in the Labrador Current. *J. Phys. Oceanogr.*, **23**, 659–678.
- Lilly, J. M., P. B. Rhines, M. Visbeck, R. Davis, J. R. N. Lazier, F. Schott, and D. Farmer, 1999: Observing deep convection in the Labrador Sea during winter 1994/95. *J. Phys. Oceanogr.*, **29**, 2065–2098.
- Maltrud, M. E., and J. L. McClean, 2005: An eddy resolving global  $1/10^\circ$  ocean simulation. *Ocean Modell.*, **8**, 31–54.
- Mathieu, P. P., 1998: Parameterization of mesoscale turbulence in a World Ocean model. Ph.D. thesis, Université catholique de Louvain, 203 pp. [Available from Institut d’Astronomie et de Géophysique G. Lemaître, Université catholique de Louvain, Chemin du cyclotron 2, B-1348, Louvain-la-Neuve, Belgium.]
- Mellor, G. L., S. Hakkinen, T. Ezer, and R. Patchen, 2002: A generalization of a sigma coordinate ocean model and an intercomparison of model vertical grids. *Ocean Forecasting: Conceptual Basis and Applications*, N. Pinardi and J. Woods, Eds., Springer, 55–72 pp.
- Myers, P. G., 2002: SPOM: A regional model of the sub-polar North Atlantic. *Atmos.–Ocean*, **40**, 445–463.
- , and A. J. Weaver, 1995: A diagnostic barotropic finite-element ocean circulation model. *J. Atmos. Oceanic Technol.*, **12**, 511–526.
- , and D. Deacu, 2004: Labrador Sea freshwater content in a model with a partial cell topographic representation. *Ocean Modell.*, **6**, 359–377.
- NOAA, 1988: Digital relief of the surface of the earth. National Geophysical Data Center Data Announcement 88-MGG-02, National Oceanic and Atmospheric Administration, Boulder, CO.
- NODC, 1994: *World Ocean Atlas CD-ROM Series 1994*. National Oceanographic Data Center, National Oceanic and Atmospheric Administration.
- Pacanowski, R. C., and S. M. Griffies, 1998: The MOM 3.0 manual. NOAA/Geophysical Fluid Dynamics Laboratory, Ocean Group Tech. Rep. 4, 680 pp.
- Rahmstorf, S., 1993: A fast and complete convection scheme for ocean models. *Ocean Modelling*, **101** (unpublished manuscripts), 9–11.
- Redi, M. H., 1982: Oceanic isopycnic mixing by coordinate rotation. *J. Phys. Oceanogr.*, **12**, 1154–1158.
- Roberts, M. J., and Coauthors, 2004: Impact of an eddy-permitting ocean resolution on control and climate change simulations with a global coupled GCM. *J. Climate*, **17**, 3–20.
- , and D. Marshall, 1998: Do we require adiabatic dissipation schemes in eddy-resolving ocean models? *J. Phys. Oceanogr.*, **28**, 2050–2063.
- Smith, R. D., M. E. Maltrud, F. O. Bryan, and M. W. Hecht, 2000: Numerical simulation of the North Atlantic Ocean at  $1/10^\circ$ . *J. Phys. Oceanogr.*, **30**, 1532–1561.
- Stammer, D., 1998: On eddy characteristics, eddy transports, and mean flow properties. *J. Phys. Oceanogr.*, **28**, 727–739.
- Stevens, D. P., 1991: The open boundary condition in the United Kingdom fine-resolution Antarctic model. *J. Phys. Oceanogr.*, **21**, 1494–1499.
- The Lab Sea Group, 1998: The Labrador Sea deep convection experiment. *Bull. Amer. Meteor. Soc.*, **79**, 2033–2058.
- Treguier, A. M., I. M. Held, and V. D. Larichev, 1997: On the parameterization of quasi-geostrophic eddies in primitive equation ocean models. *J. Phys. Oceanogr.*, **27**, 567–580.
- Trenberth, K. R., W. G. Large, and J. G. Olson, 1990: The mean annual cycle in global ocean wind stress. *J. Phys. Oceanogr.*, **20**, 1742–1760.
- Visbeck, M., J. Marshall, T. Haine, and M. Spall, 1997: Specification of eddy transfer coefficients in coarse-resolution ocean models. *J. Phys. Oceanogr.*, **27**, 381–402.
- Willebrand, J., and Coauthors, 2001: Circulation characteristics in three eddy-permitting models of the North Atlantic. *Progress in Oceanography*, Vol. 48, Pergamon, 123–161.
- Wright, D. K., 1997: A new eddy mixing parametrization and ocean general circulation model. *International WOCE Newsletter*, No. 26, WOCE International Project Office, Southampton, United Kingdom, 27–29.